



Article

Numerical Simulation and Experiment of Dust Suppression Device of Peanut Whole-Feed Combine Using Computational Fluid Dynamics

Hongbo Xu ^{1,2} , Peng Zhang ² , Fengwei Gu ², Zhichao Hu ², Hongguang Yang ², Enrong Mao ^{1,*} and Yuefeng Du ¹

¹ College of Engineering, China Agricultural University, Beijing 100083, China

² Nanjing Institute of Agricultural Mechanization, Ministry of Agriculture and Rural Affairs, Nanjing 210014, China

* Correspondence: gxy15@cau.edu.cn

Abstract: Peanut whole-feed combines discharge a large amount of dust while harvesting, causing serious air pollution and detrimental environmental change. To reduce the dust emission from peanut whole-feed combines, a cyclone separation dust suppression device for peanut whole-feed combines was proposed in this study. A three-dimensional computational fluid dynamics (CFD) model coupled with dust particles and dust emission airflow was established to simulate the effect of a dust suppression device on capturing dust particles. Then, the effectiveness of the dust suppression device was verified by a dust suppression test system on a peanut whole-feed combine. The results show that when the inlet wind velocity of the dust suppression device increased from 15 m/s to 25 m/s, the separation efficiency of the measured value fluctuated between 90.79% and 96.07%, while the simulated value fluctuated between 95.18% and 96.59%. Moreover, the particle size of the discharged dust particles was significantly reduced under the action of the dust suppression device. The discharged dust particle size constant of the measured value was 8.6 μm , while the simulated value was 5.1 μm . The study methods and results can provide a reference for the dust suppression optimization of peanut whole-feed combines and similar agricultural machines.

Keywords: dust suppression; peanut whole-feed combine; separation efficiency; size distribution; computational fluid dynamics



Citation: Xu, H.; Zhang, P.; Gu, F.; Hu, Z.; Yang, H.; Mao, E.; Du, Y. Numerical Simulation and Experiment of Dust Suppression Device of Peanut Whole-Feed Combine Using Computational Fluid Dynamics. *Agriculture* **2023**, *13*, 329. <https://doi.org/10.3390/agriculture13020329>

Academic Editor: Jacopo Bacenetti

Received: 31 December 2022

Revised: 18 January 2023

Accepted: 27 January 2023

Published: 29 January 2023



Copyright: © 2023 by the authors. Licensee MDPI, Basel, Switzerland. This article is an open access article distributed under the terms and conditions of the Creative Commons Attribution (CC BY) license (<https://creativecommons.org/licenses/by/4.0/>).

1. Introduction

Peanut whole-feed harvesting is the most widely used mechanized peanut harvest mode in the world with the advantages of low operation cost and high efficiency [1–3]. During peanut whole-feed harvest, peanut plants with entrained soil are separated into pods and stalk residuals under the action of the working components, but at the same time, a large amount of dust is also produced and discharged out of the machines [4]. Dust pollution produced by agricultural mechanization is of increasing concern because of its damage to the surrounding environment and neighboring residents' health [5–7], and thus, the diffusion of dust discharged from peanut whole-feed combines has attracted the attention of scholars. Previous studies have identified the basic characteristics and potential hazard forms of dust emissions from peanut combined harvesting operations [4,8]. The concentration of dust discharged from peanut combines is relatively high, mainly because peanut plants contain a lot of soil. How to reduce dust emissions during the operation process has become the latest research focus.

Several studies have been conducted on dust suppression of crop combine harvesters. Baticados et al. evaluated the potential emission reduction from using low-dust harvesters for almond nut-picking operations compared with the conventional harvester using the American Meteorological Society/Environmental Protection Agency Regulatory Model [9].

Guofeng et al. analyzed the effects of the storage cage structure, flow velocity at the duct outlet, ambient wind velocity, and particle size on dust emissions of a mobile straw granulator to control the dust emissions and reduce the mass ratio of the dust into the press device of the granulator [10]. Kruckman developed a combine dust eliminator attachable to the feeder housing of a John Deere combine without modifying the feeder housing [11]. Law et al. presented the theoretical basis, including relevant mass- and charge-balances, for electrostatically abating the PM_{2.5} airborne dust from mechanized tree-nut harvesting [12]. However, dust suppression technology and methods for peanut whole-feed combines are still insufficient.

Spray dust suppression technology is widely used in mining, construction, and other fields because of its low cost and high efficiency, and has also been adopted by some peanut combine manufacturers [13]. However, it requires continuous water supply, which affects the normal operation progress of peanut harvesting machinery [14]. Therefore, this method had not been recognized by the market because it increases the burden on producers. A cyclone separator uses centrifugal force to separate particles and gas, and the separation efficiency can reach more than 90% under appropriate working parameters [15]. However, due to the lack of a design basis and evaluation method, this equipment is still in the exploration stage for dust suppression during peanut combine operation.

Numerical simulation methods are effective means for the research of dust suppression technology [16–18]. By using computational fluid dynamics (CFD) technology, the separation performance of cyclone separators with different structures under various operating parameters can be quickly explored [19]. Although the numerical simulation of the working process of the cyclone separator is relatively mature, there is no specific study on the application of the cyclone separator to the dust suppression of peanut whole-feed combines.

In this study, a cyclone separation dust suppression device was designed according to the dust characteristics of peanut whole-feed combines, and the dust suppression performances were simulated and tested. This study provides an effective dust suppression device and its evaluation method for peanut whole-feed combines, and provides a reference for the optimization of dust suppression of similar agricultural machines.

2. Materials and Methods

2.1. Description of Dust Suppression Device for the Peanut Whole-Feed Combine

As shown in Figure 1, the peanut whole-feed combine used for our study is widely used in agriculture in China. Peanut plants are separated into pods and stalks under the action of the working parts of the harvester, but at the same time, a large amount of dust is also produced, which is discharged from the rear of the stalk gathering tank along with the dust exhaust airflow. To reduce the dust emission from the combine, a vehicle-mounted cyclone separation dust suppression device is designed in this study. The dust suppression device is composed of two cyclone separators rotating in opposite directions in parallel, and is installed at the tail of the combine. The air inlet of the dust suppression device faces the dust outlet of the combine.

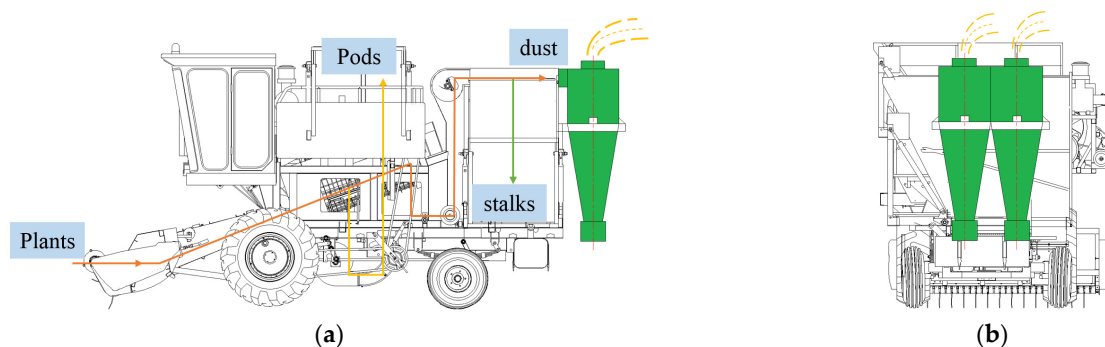


Figure 1. Diagrams of peanut whole-feed combine with a dust suppression device: (a) side view; (b) rear view.

As shown in Figure 2, when the dusty air flow enters the cyclone separator, the dust and air are separated under the action of centrifugal force. The clean air is discharged from the top of the cyclone separator, while the dust settles into the dust collection bucket at the bottom of the cyclone separator under the action of gravity and is cleaned by an air-lock valve periodically [20]. The key dimensions of the cyclone separator used in this study are summarized in Table 1.

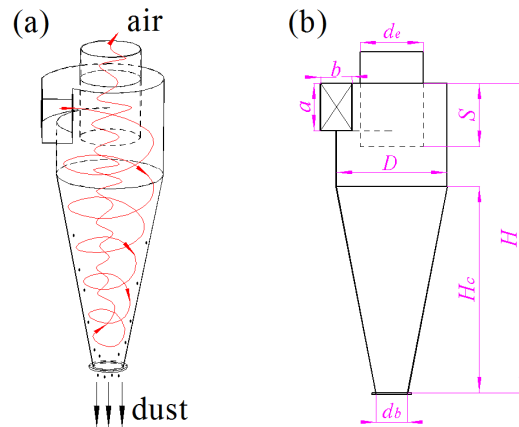


Figure 2. Image of (a) working principle and (b) structure of the cyclone separator.

Table 1. Key dimensions of the cyclone separator.

Index	Symbol	Value
Diameter of cylinder (mm)	D	700
Height of cylinder (mm)	H	1950
Height of cone (mm)	H_c	1300
Depth of exhaust pipe (mm)	S	400
Height of intake pipe (mm)	a	300
Width of intake pipe (mm)	b	200
Diameter of exhaust pipe (mm)	d_e	400
Diameter of dust collection bucket (mm)	d_b	200

2.2. CFD Analysis

2.2.1. Mathematical Model

The continuous gas phase is treated in the Euler coordinate system. The Reynolds stress equation model (RSM) completely discards the assumption based on isotropic eddy viscosity, and more strictly considers streamline bending, vortex, rotation, and rapid change of tension [21]. It has the potential to predict complex flows with higher accuracy, and can better reflect the true situation of the internal flow field of the cyclone separator. Although it consumes more computing resources, the existing computer processing capacity fully meets its computing needs. In the Reynolds stress equation, k and ϵ are calculated as follows [22]:

$$\frac{\partial}{\partial t}(\rho k) + \frac{\partial}{\partial x_i}(\rho k u_i) = \frac{\partial}{\partial x_j} \left[\left(\mu + \frac{\mu_t}{\sigma_k} \right) \frac{\partial k}{\partial x_j} \right] + \frac{1}{2}(P_{ii} + G_{ii}) - \rho \epsilon (1 + 2M_t^2) + S_k \quad (1)$$

$$\frac{\partial}{\partial t}(\rho \epsilon) + \frac{\partial}{\partial x_i}(\rho \epsilon u_i) = \frac{\partial}{\partial x_j} \left[\left(\mu + \frac{\mu_t}{\sigma_\epsilon} \right) \frac{\partial \epsilon}{\partial x_j} \right] + C_{\epsilon 1} \frac{1}{2}(P_{ii} + C_{\epsilon 3} G_{ii}) \frac{\epsilon}{k} - C_{\epsilon 2} \rho \frac{\epsilon^2}{k} + S_\epsilon \quad (2)$$

where k is the turbulent kinetic energy, m^2/s^2 ; ϵ is the turbulent energy dissipation rate, m^2/s^3 ; ρ is the gas density, kg/m^3 ; u is the velocity in the x direction, m/s ; i, j is the indicator symbol; μ is laminar viscosity, $kg/(m \cdot s)$; μ_t is turbulent viscosity, $kg/(m \cdot s)$; T is the time, s ; P_{ij} is shear stress generation term, Pa/s ; G_{ij} is the buoyancy generation term, Pa/s ; M_t

is the turbulent Mach number, among other coefficients, $\sigma_k = 1.0$, $\sigma_\epsilon = 1.0$, $C_{\epsilon 1} = 1.44$, and $C_{\epsilon 2} = 1.92$; $C_{\epsilon 3}$ is the flow property coefficient of a point relative to gravity; and S_k and S_ϵ are user-defined source items.

Discrete particle phase is treated in the Lagrangian coordinate system. The force balance equation of a single particle can be obtained from Newton's second law, expressed as [23]:

$$\frac{d\vec{u}_p}{dt} = \frac{\vec{u} - \vec{u}_p}{\tau_r} + \frac{\vec{g}(\rho_p - \rho)}{\rho_p} + \vec{F} \quad (3)$$

where u_p is the particle velocity, m/s; u is the gas velocity, m/s; g is the acceleration of gravity, m/s²; ρ_p is the particle density, kg/m³; ρ is the gas density, kg/m³; F is the additional acceleration term, m/s², such as the acceleration of particles caused by pressure gradient force, thermophoresis force, Saffman lift, etc., which is usually negligible compared with the drag force; and τ_r is the particle relaxation time, expressed as

$$\tau_r = \frac{\rho_p d_p^2}{18\mu} \cdot \frac{24}{C_d R_e} \quad (4)$$

where d_p is the particle diameter, m; μ is laminar viscosity, kg/(m·s); C_d is the resistance coefficient, given by different relative Reynolds number ranges; and R_e is the relative Reynolds number, expressed as

$$R_e = \frac{\rho d_p |\vec{u}_p - \vec{u}|}{\mu} \quad (5)$$

After the force balance equation of particles is obtained, the trajectory of the particles can be predicted by integrating the particle velocity vector in time.

2.2.2. Model and Boundary Conditions

CFD simulations were performed using commercial CFD software (Fluent, Ver. 2019 R1, Ansys Inc., Canonsburg, PA, USA). The 3D problem domain was established based on the interior of the cyclone separator, but the length of the exhaust pipe was extended slightly to prevent particles from leaving the calculation domain in less than a time step. As shown in Figure 3, a polyhedron mesh with 158,992 elements and 559,248 nodes was adopted for the computational domain. The biggest advantage of the polyhedron mesh is that it has many adjacent elements, so it can more accurately calculate the gradient of the control volume. Even at the edges and corners, the polyhedral mesh usually has multiple neighbor elements, so that the gradient and local flow distribution can be calculated normally. In addition, the mesh quality analysis showed that the maximum skewness metric of this model is 0.758, so the gridding quality is acceptable.

Gravitational acceleration was set of 9.81 m/s² with an atmospheric pressure of 101,325 Pa. The inlet boundary condition was set to the velocity inlet type while the outlet condition was set to the pressure outlet. The inlet wind velocity was set as 15~25 m/s to correspond with different test conditions. The hydraulic diameter of the inlet and outlet was set at 0.24 and 0.36 m, respectively. The Reynolds stress equation model (RSM) was chosen for the simulations because it has higher prediction accuracy for complex flows and has been widely used in many cyclone separator studies [24].

In the simulation domain, the no-slip wall condition was used for all the cyclone separator walls. The DPM boundary condition of the side wall and underside wall was set as reflect and trap, respectively, which means that the dust particles would stop moving when arriving at the bottom of the cyclone separator. Moreover, the DPM boundary condition of the outlet face was set to escape, which means that the uncaptured particles would escape from the top of the cyclone separator.

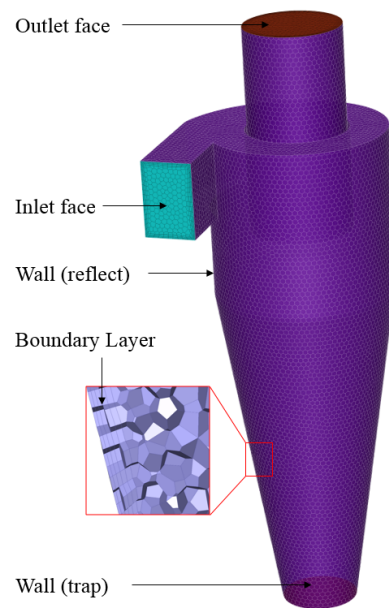


Figure 3. The shape and distribution of elements in the computational domain.

2.2.3. Discrete Phase Model

The discrete phase model was activated to simulate the movement of dust particles, which interacted with the continuous phase (dust emission airflow) every ten time steps. Characteristics of dust particles including concentration, size distribution, shape factor, and true density were detected using the equipment and method in Reference [8]. The dust concentration was obtained using a filter membrane weighing method (GBZ/T 192.1-2007) and was calculated using the following equation [25]:

$$c = \frac{m_2 - m_1}{V \times t} \times 1000 \quad (6)$$

where c is the concentration of dust in the air (mg/m^3), m_2 is the quality of the filter membrane after sampling (mg), m_1 is the quality of the filter membrane before sampling (mg), V is the sampling flow rate (L/min), and t is the sampling time (min).

The total flow rate of dust at the outlet is as follows:

$$Q = \frac{S \cdot c \cdot v_f}{10^6} \quad (7)$$

where Q is the total flow rate of the dust (mg/s), S is the dimension of the dust outlet (mm), c is the concentration of dust at the outlet (mg/m^3), and v_f is the dust particle speed at the dust outlet (m/s).

To ensure the accuracy of numerical simulation, the physical parameters of the dust particles were obtained through experimental measurements, and the dust particle size was divided into two groups: 1–10 μm and 11–310 μm , respectively, in order to display the numerical simulation results more clearly. These two dust groups accounted for 22.91% and 77.09% of the total flow rate of dust, respectively [8]. The parameters for the discrete phase model are summarized in Table 2. The effects of the Saffman lift force, virtual mass force, and pressure gradient force were considered.

2.2.4. Solution Methods and Simulation Procedure

The SIMPLEC (semi-implicit method for pressure linked equation consistent) algorithm was used under the pressure–velocity coupling scheme. The least square cell based PRESTO! (pressure staggering option) and QUICK (quadratic upwind interpolation for convective kinematics) schemes were used for the spatial discretization of gradient, pressure, and momentum equations, respectively, to achieve higher accuracy [26].

The escaping particles may stay in the computational domain for a very short time, thus the time step was set to 0.001 s. All the simulations were run in parallel processing with a 64-core dual Intel(R) Xeon(R) Gold 6248R, 3.0 GHz, with 128 GB memory.

Table 2. Discrete phase parameters used in the simulations.

Dust Group	Property	Value	Sources
	Total flow rate of dust ($\text{mg}\cdot\text{s}^{-1}$)	9513.7	Calculated by Equation (7)
	Temperature (K)	300	Measured by temperature sensor
	Ture density of dust ($\text{g}\cdot\text{cm}^{-3}$)	2.5277	Measured by automatic true density analyzer
1	Flow rate of dust ($\text{mg}\cdot\text{s}^{-1}$)	2179.6	Calculated by Ref. [8]
	Min. diameter of dust (μm)	1	Measured by laser particle size analyzer
	Max. diameter of dust (μm)	10	Measured by laser particle size analyzer
	Size constant of dust (μm)	7.3	Estimated by Rosin–Rammmler curve fit
	Spread parameter of dust	2.76	Calculated by Ref. [8]
2	Flow rate of dust ($\text{mg}\cdot\text{s}^{-1}$)	7334.1	Calculated by Ref. [8]
	Min. diameter of dust (μm)	11	Measured by laser particle size analyzer
	Max. diameter of dust (μm)	310	Measured by laser particle size analyzer
	Size constant of dust (μm)	27.5	Estimated by Rosin–Rammmler curve fit
	Spread parameter of dust	1.35	Calculated by Ref. [8]

When the residual of numerical simulation converged, the mass of escaped particles could be counted through the “Mass Transfer Summary” function at the outlet face. Thus, the simulation value of separation efficiency could be calculated by the following equation:

$$\varnothing_s = \left(1 - \frac{\Delta m / \Delta t}{Q}\right) \times 100\% \quad (8)$$

where \varnothing_s is the simulation value of the separation efficiency of the dust suppression device (%); Δm is the mass of escaped particles in the simulation time (mg); Δt is the simulation time (s); and Q is the total flow rate of the dust (mg/s).

2.3. Model Validation Test

2.3.1. Dust Suppression Test System

To verify the working performance of the dust suppression device, it is necessary to carry out the dust suppression test on the process of peanut whole-feed harvest. Considering the test cost and the feasibility of operation, a dust suppression test system for a peanut whole-feed combine was designed in this study. As shown in Figure 4, the dust suppression test system was composed of two parallel cyclone separators (the key dimensions are summarized in Table 1) and a pulse jet filter cartridge dust collector (XFLT-81, Jinan Xufeng Environmental Protection Machinery Equipment Co., Ltd., Jinan China) in series. The inlet of the dust suppression test system, that is, the inlet of the parallel cyclone separators, was connected with the dust outlet of the peanut whole-feed combine, and an integrated atmospheric sampler (KB-120F, Qingdao Genstar Electronic Technology Co., Ltd., Qingdao, China) was set at the exhaust outlet of the pulse jet filter cartridge dust collector. Cyclone separators and a pulse filter cartridge dust collector were independently driven by a variable frequency motor, which could match the dust exhaust air volume of the peanut whole-feed combine. The air volume value of each component at different speeds refers to the fan manual.

Under the action of the dust suppression system, the dust discharged from the peanut whole-feed combine entered two parallel cyclone separators for primary collection, and the collected dust entered the dust collection bucket below the cyclone separator. The residual dust escaped from the cyclone separator and entered the pulse jet filter cartridge dust collector for secondary collection, and the collected dust fell into the dust box at the bottom of the dust collector under the action of pulse air flow. The residual dust on the surface of

the filter cartridge was cleaned into the dust box with a brush. In addition, the dust passing through the filter cartridge was collected and measured by an integrated atmospheric sampler that was set beside the outlet of the pulse jet filter cartridge dust collector, and the measurement method refers to the standard literature (GBZ/T 192.1-2007) [25].

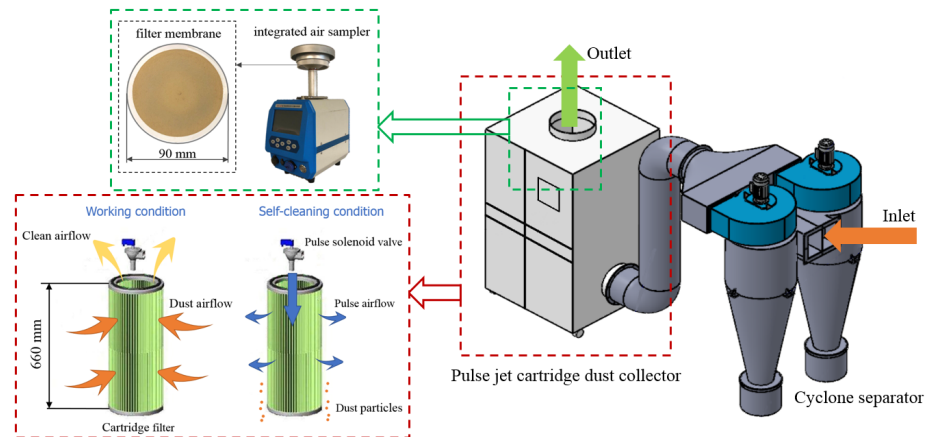


Figure 4. Schematic diagram of the dust suppression test system.

By using the dust suppression test system, the dust suppression efficiency and particle size change in the dust suppression device of the peanut whole-feed combine could be accurately measured. At the same time, it reduced the cost and time of the integrated design of the peanut combine and dust suppression device. Because the dust suppression test system required a stable power supply and was difficult to move during operation, an indoor simulation test was carried out instead of a field test in this study.

2.3.2. Measurement of Separation Efficiency and Particle Size

The dust collected by the cyclone separators was mixed with some peanut stalk debris. Therefore, it was necessary to screen the collected dust with a 355 μm analytical sieve to remove short stems and leaves. The separation efficiency of the dust suppression device of the peanut whole-feed combine is provided as follows:

$$\varnothing = \frac{m_1}{m_1 + m_2 + c \times F_a \times t} \times 100\% \quad (9)$$

where \varnothing is the separation efficiency of the dust suppression device of the peanut whole-feed combine (%), m_1 is the mass of dust collected by cyclone separators (mg), m_2 is the mass of dust collected by the pulse jet filter cartridge dust collector (mg), c is the concentration of dust after the collection of the dust suppression test system (mg/m^3), F_a is the air flow rate of the dust suppression test system (m^3/min), and t is the feeding time (min).

In addition, a laser particle size analyzer (Mastersizer 2000, Malvern Instruments Ltd., Worcestershire, UK) was used to measure the particle size distribution of the dust in the dust box of the pulse jet filter cartridge dust collector. This measurement could reflect the characteristics of particle size captured and discharged by the dust suppression device of the peanut whole-feed combine. The particle size distribution of dust particles in the collector was described using the Rosine–Rammler curve fit [27].

2.3.3. Experiment Condition

The experiment of the dust suppression test system was carried out in Suiping County, Zhumadian City, Henan Province, in September 2021. The peanuts (No.2 Wanhua) used in the test include pods, stalks, and entrained soil; the proportion and dry basis moisture content of each component of peanut material were measured by electronic balance and a drying box (105 $^{\circ}\text{C}$ drying method). Measurement results showed that the proportion of pods, stalks, and entrained soil accounted for 44.63%, 38.49%, and 16.88% respectively,

while the moisture content of pods, stalks, and entrained soil accounted for 16.38%, 19.81%, and 4.83% respectively.

During the test, the peanut whole-feed combine and the dust suppression test system were started at the same time. After that, the engine speed of the peanut whole-feed combine was adjusted to the rated working speed, and the fan speed of the cyclone separators and pulse jet filter cartridge dust collector were adjusted to make the air inlet of the dust suppression system equal to the air exhaust of the combine. Then, the prepared peanut plant materials were fed manually to the peanut whole-feed combine (Figure 5). After the test, dust in the dust collection bucket of the cyclone separator and in the pulse jet filter cartridge dust collector were collected, respectively.



Figure 5. Experiment of the dust suppression test system.

The test was carried out at 5 different wind velocities at the dust outlet of the peanut whole-feed combine, respectively (15 m/s, 17.5 m/s, 20 m/s, 22.5 m/s, and 25 m/s), by adjusting the engine speed. The air volume collected by the dust suppression test system was adjusted to be consistent with the air volume of the dust emission from the peanut whole-feed combine. The air volume of the dust emission from the peanut whole-feed combine was calculated by the following equation:

$$L = 3600 \times F \times v_w \quad (10)$$

where L is the air volume of the dust emission from the peanut whole-feed combine (m^3/h); F is the area of dust outlet (m^2); and v_w is the wind velocity at dust outlet (m/s). After the combine and the dust suppression test system were running stably, 250 kg of materials were fed manually for each test. After the test, dust in the dust collection bucket of the cyclone separation dust suppression device was collected. A total of 5 groups of tests were conducted, and each test was repeated 3 times. The test was not affected by the environment because the temperature and humidity during the test were basically the same as the actual operation, and the atmospheric flow did not affect the operation of the dust suppression device, so the influence of environmental variables on the test could be ignored. The separation efficiency of the dust suppression device could be obtained by weighing the collected dust with an electronic balance and calculating the average value. The test settings are shown in Table 3.

Table 3. Setting of test parameters.

Test No.	Engine Speed/rpm	Wind Velocity/($\text{m}\cdot\text{s}^{-1}$)	Peanut Plants Weight/kg
T1	1500	15.0	250
T2	1750	17.5	250
T3	2000	20.0	250
T4	2250	22.5	250
T5	2500	25.0	250

3. Results

3.1. Analysis of Simulation Results

Figure 6a shows the Z-direction air flow velocity in the cyclone separator when the inlet wind velocity was 20 m/s. It can be seen from Figure 6a that when the gas entered the cyclone separator, the cyclone was formed due to the restriction of the cyclone separator wall. Tangential velocity played a leading role in the cyclone separator, which was conducive to throwing dust particles to the wall and capturing them. The surface of maximum tangential velocity was cylindrical, and the radius was related to the ground inner diameter of the cyclone separator.

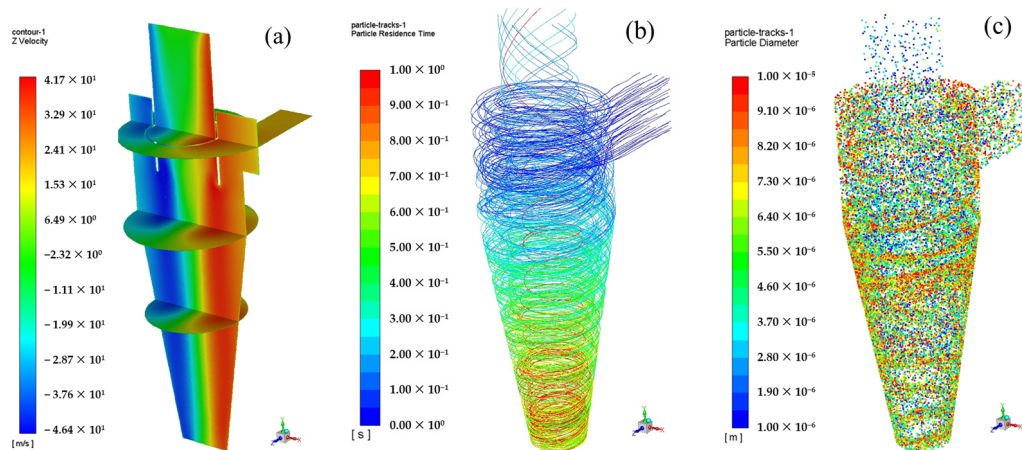


Figure 6. Simulation results (inlet wind velocity was 20 m/s): (a) Z-direction air flow velocity; (b) particle tracks by residence time; and (c) spatial distribution of dust particle diameter.

Due to the different particle diameters and incident positions of dust particles, the particle trajectory of particles also varied significantly (Figure 6b). Most particles reached the bottom of the cyclone separator under the action of the external cyclone within 0.7 s, while a small amount of particles would enter the exhaust pipe and exit the cyclone separator with the internal cyclone. Due to the impact of the incident position and particle size, particles may enter the exhaust pipe directly, or be entrained by the internal vortex flow at the bottom of the cyclone separator and escape from the cyclone separator. The particles from the inside of the inlet were easier to escape than those from the outside because the centrifugal force of the inside particles was smaller than that of the outside particles, so they were more vulnerable to the impact of the upwardly moving inner vortex flow. Dust particles with different diameters also have different motion modes in the cyclone separator. The particle size of the discharged particles from the cyclone separator was mainly 0~10 μm (Figure 6c), which showed that particles with larger particle sizes are easier to be captured. This finding is consistent with the work by Wan et al. [28].

The numerical simulation results showed that the cyclone separator has a reasonable structure, which can achieve the dust suppression effect for the peanut whole-feed combine.

3.2. Analysis of Separation Efficiency

The separation efficiency of the numerical simulation was compared with the experimental results. These results, presented in Figure 7, show that the measured value was slightly lower than the simulated value with relative errors less than 5%. This phenomenon may be caused by the selection of boundary conditions during the simulation calculation. It is believed that the particles can be trapped once they collide with the cone wall of the cyclone separator. However, as a matter of fact, the small particles that already hit the wall may return to the gas flow field under the action of some small vortices on the wall, and some of them will re-enter the updraft to escape at the outlet, which leads to a simulated value of separation efficiency greater than the experimental value.

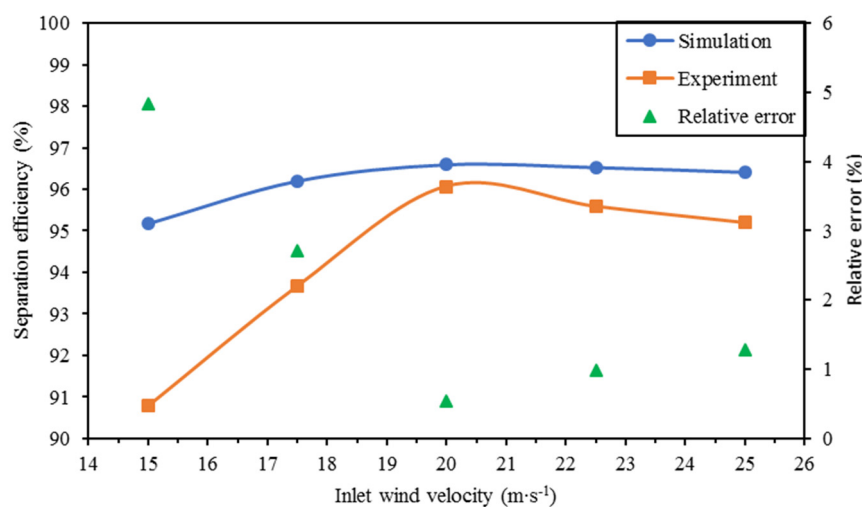


Figure 7. Separation efficiency of dust suppression device with different wind velocity.

When the inlet wind velocity increased from 15 m/s to 20 m/s, the separation efficiency of both the measured value and the simulated value was increased. The measured value increased from 90.79% to 96.07%, while the simulated value increased from 95.18% to 96.59%. This is because the increase in centrifugal force is conducive to the separation of particles and gas. Conversely, when the inlet wind velocity increased from 20 m/s to 25 m/s, the separation efficiency of both the measured value and the simulated value was slightly decreased. The measured value decreased from 96.07% to 95.19%, while the simulated value decreased from 96.59% to 96.41%. This may be due to the enhanced turbulence disturbance which makes the back-mixing more severe. The maximum relative error between the measured value and the simulated value was 4.83%, so the established dust suppression simulation model could perhaps be deemed accurate and reliable enough to illustrate the capacity of the cyclone separator.

The established CFD model made it more clear to understand the movement state of particles with different components and different particle sizes under the action of the dust suppression device, which was conducive to the evaluation of the performance of the dust suppression device, and provided convenient verification means for the structural optimization of the dust suppression device. At the same time, the modeling method of this study could be used for the evaluation and matching design of similar dust suppression devices of other crop harvesting machines, such as the design of dust suppression devices for wheat combines.

In the working range, the actual separation efficiency of the dust suppression device of the peanut whole-feed combine was more than 90%, which showed that it can effectively reduce the dust emission pollution of the combine. In our future study, the integrated design of the dust suppression device and the peanut whole-feed combine will be completed, and further performance tests will be carried out in the field.

3.3. Analysis of Particle Size Distribution

As the particle size distribution does not change significantly under different wind velocities according to the test results of the laser particle size analyzer, this study only shows the simulation and test results of the dust particle size input to the dust suppression device and its output when the inlet wind velocity was 20 m/s; the results are shown in Figure 8. It can be seen that both the simulation results and the test results show that the particle size of the discharged dust particles was significantly reduced under the action of the dust suppression device. The simulation results show that the size constant of the discharged dust particles was 5.1 μm , while the test results show that the size constant of the discharged dust particles was 8.6 μm . The test value of the particle size of the discharged dust particles was larger than the simulation value, which may be due to the

fact that there were not only soil particles but also fiber particles mixed in the discharged dust particles, and the particle size of the fiber particles was much larger than that of soil particles [29]. However, the proportion and particle size characteristics of the fiber particles were not measured, so the influence of fiber particles on the dust discharged from the dust suppression device was ignored in the numerical simulation, resulting in the test value of the particle size of the actual discharged dust being greater than the simulation value.

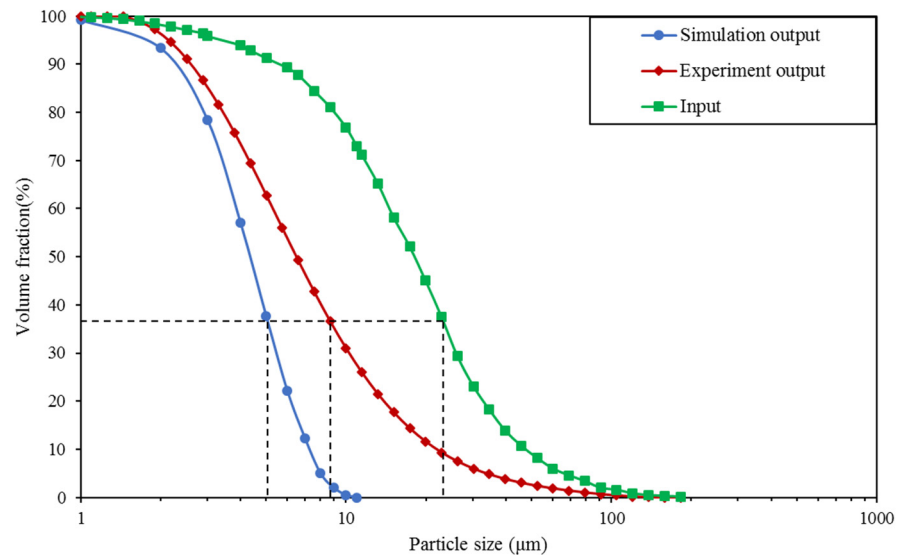


Figure 8. Cumulative size distribution of dust particles escaping from the dust suppression device when the inlet wind velocity was 20 m/s under the Rosine–Rammmler mathematical distribution. (The particle size constant is the particle size when the cumulative volume fraction is 36.8%).

Although the dust suppression device significantly reduced the dust concentration discharged from the peanut whole-feed combine, the particle size analysis shows that the dust suppression device mainly captured particles with larger particle sizes, while particles with smaller particle sizes were more likely to enter the human body and had a greater impact on human health [30,31]. Therefore, how to further inhibit the emission of smaller particles is one of the important directions in our future study.

4. Conclusions

To reduce dust pollution from peanut whole-feed combines, a cyclone separation dust suppression device was designed according to the dust characteristics of a peanut whole-feed combine and a dust suppression model was established via CFD. On this basis, the dust suppression performances were simulated and tested. The results show that when the inlet wind velocity increased from 15 m/s to 25 m/s, the separation efficiency of the measured value fluctuated between 90.79% and 96.07%, while the simulated value fluctuated between 95.18% and 96.59%. The relative error between the measured value and the simulated value was below 5%. Moreover, the particle size of the discharged dust particles was significantly reduced under the action of the dust suppression device. The discharged dust particle size constant of the measured value was 8.6 μm, while the simulated value was 5.1 μm.

Through the numerical simulation and experiment, we found that the cyclone separation dust suppression device could significantly reduce the dust emission concentration from the peanut whole-feed combine with its reasonable structure. Conversely, this modeling method could be used to predict the separation efficiency of a similar dust suppression device for peanut whole-feed combines and other farmland machinery.

Due to the limitation of experiment costs, this study only carried out a site simulation test. In the future study, the integrated design of the dust suppression device and the

peanut whole-feed combine will be carried out and field tests will be conducted for further improvement of the dust suppression device.

Author Contributions: Conceptualization, H.X. and P.Z.; methodology, P.Z.; software, Y.D.; validation, H.X., P.Z. and Z.H.; formal analysis, Y.D.; investigation, F.G.; resources, P.Z.; data curation, Z.H.; writing—original draft preparation, H.X.; writing—review and editing, E.M.; visualization, F.G. and H.Y.; supervision, E.M.; project administration, Z.H.; funding acquisition, Z.H. All authors have read and agreed to the published version of the manuscript.

Funding: This research was funded by the Central Public-interest Scientific Institution Basal Research Fund, grant number S202233, and the China Postdoctoral Science Foundation, grant number 2021M7018020.

Institutional Review Board Statement: Not applicable.

Informed Consent Statement: Not applicable.

Data Availability Statement: The datasets used and/or analyzed during the current study are available from the corresponding author on reasonable request.

Acknowledgments: The authors would like to acknowledge Henan Nongyouwang Agricultural Equipment Technology Co., Ltd., Henan China, for providing the test materials and site for this study.

Conflicts of Interest: The authors declare no conflict of interest.

References

- Chen, Z.; Gao, L.; Chen, C.; Butts, C.L. Analysis on technology status and development of peanut harvest mechanization of China and the United States. *Trans. Chin. Soc. Agric. Mach.* **2017**, *48*, 1–21.
- Zhang, P.; Xu, H.; Zhuo, X.; Hu, Z.; Lian, C.; Wang, B. Biotribological characteristic of peanut harvesting impact-friction contact under different conditions. *Agronomy* **2022**, *12*, 1256. [[CrossRef](#)]
- Yang, H.; Cao, M.; Wang, B.; Hu, Z.; Xu, H.; Wang, S.; Yu, Z. Design and test of a tangential-axial flow picking device for peanut combine harvesting. *Agriculture* **2022**, *12*, 179. [[CrossRef](#)]
- Zhang, P.; Xu, H.; Hu, Z.; Chen, Y.; Cao, M.; Yu, Z.; Mao, E. Characteristics of Agricultural Dust Emissions from Harvesting Operations: Case Study of a Whole-Feed Peanut Combine. *Agriculture* **2021**, *11*, 1068. [[CrossRef](#)]
- Chen, W.; Tong, D.Q.; Zhang, S.; Zhang, X.; Zhao, H. Local PM10 and PM2.5 emission inventories from agricultural tillage and harvest in northeastern China. *J. Environ. Sci.* **2017**, *57*, 15–23. [[CrossRef](#)] [[PubMed](#)]
- Schenker, M. Exposures and Health Effects from Inorganic Agricultural Dusts. *Environ. Health Perspect.* **2000**, *108*, 661–664.
- Zhou, L.; Chen, X.; Tian, X. The impact of fine particulate matter (PM2.5) on China's agricultural production from 2001 to 2010. *J. Clean. Prod.* **2018**, *178*, 133–141. [[CrossRef](#)]
- Xu, H.; Zhang, P.; Hu, Z.; Mao, E.; Yan, J.; Yang, H. Analysis of dust diffusion from a self-propelled peanut combine using computational fluid dynamics. *Biosyst. Eng.* **2022**, *215*, 104–114. [[CrossRef](#)]
- Baticados, E.; Capareda, S.; Maglinao, A. Particulate matter emission factors using low-dust harvesters for almond nut-picking operations. *J. Air Waste Manag. Assoc.* **2019**, *69*, 1304–1311. [[CrossRef](#)]
- Guofeng, W.; Yuanjuan, G.; Dezhi, R.; Zhao, J.; Xuewei, B. Research on dust control of mobile straw granulator. *Comput. Electron. Agric.* **2021**, *189*, 106375. [[CrossRef](#)]
- Kruckman, H.D. Combine dust eliminator. U.S. Patent US6036600 A, 14 March 2000.
- Law, S.E.; Giles, D.K. Electrostatic abatement of airborne respirable dust emission from mechanized tree-nut harvesting: Theoretical basis. *J. Electrostat.* **2009**, *67*, 84–88. [[CrossRef](#)]
- Yang, M. A Dust Removal Device for Agricultural Machinery. CN2018203303457, 16 April 2019.
- Liu, Y.; Shao, L.; Wang, W.; Chen, J.; Zhang, H.; Yang, Y.; Hu, B. Study on Fugitive Dust Control Technologies of Agricultural Harvesting Machinery. *Agriculture* **2022**, *12*, 1038. [[CrossRef](#)]
- Cai, J.; Wang, Z.; Jin, Y.; Lyu, J.; Yang, H. Analysis of Gas-solid Flow Distribution in Double Identical Parallel Cyclones. *Proc. CSEE* **2019**, *39*, 2106–2113.
- Wang, P.; Tan, X.; Zhang, L.; Li, Y.; Liu, R. Influence of particle diameter on the wettability of coal dust and the dust suppression efficiency via spraying. *Process Saf. Environ. Prot.* **2019**, *132*, 189–199. [[CrossRef](#)]
- Li, S.; Zhao, B.; Lin, H.; Shuang, H.; Kong, X.; Yang, E. Review and prospects of surfactant-enhanced spray dust suppression: Mechanisms and effectiveness. *Process Saf. Environ. Prot.* **2021**, *154*, 410–424. [[CrossRef](#)]
- Zhou, Q.; Qin, B. Coal dust suppression based on water mediums: A review of technologies and influencing factors. *Fuel* **2021**, *302*, 121196. [[CrossRef](#)]
- Cortés, C.; Gil, A. Modeling the gas and particle flow inside cyclone separators. *Prog. Energy Combust. Sci.* **2007**, *33*, 409–452. [[CrossRef](#)]
- Gawali, S.S.; Bhambere, M.B. Effect of design and the operating parameters on the performance of cyclone separator—a review. *Int. J. Mech. Eng. Rob. Res.* **2015**, *4*, 244–248.

21. Durbin, P. A Reynolds stress model for near-wall turbulence. *J. Fluid Mech.* **1993**, *249*, 465–498. [[CrossRef](#)]
22. Wallin, S.; Johansson, A. An explicit algebraic Reynolds stress model for incompressible and compressible turbulent flows. *J. Fluid Mech.* **2000**, *403*, 89–132. [[CrossRef](#)]
23. Feng, Y.Q.; Yu, A.B. Assessment of Model Formulations in the Discrete Particle Simulation of Gas–Solid Flow. *Ind. Eng. Chem. Res.* **2004**, *43*, 8378–8390. [[CrossRef](#)]
24. Wang, B.; Xu, D.L.; Chu, K.W.; Yu, A.B. Numerical study of gas–solid flow in a cyclone separator. *Appl. Math. Model.* **2006**, *30*, 1326–1342. [[CrossRef](#)]
25. GBZ/T 192.1; Determination of Dust in the Air of Workplace. Part 1: Total Dust Concentration. Standardization Administration of the People’s Republic of China: Beijing, China, 2007.
26. Elsayed, K.; Lacor, C. Optimization of the cyclone separator geometry for minimum pressure drop using mathematical models and CFD simulations. *Chem. Eng. Sci.* **2010**, *65*, 6048–6058. [[CrossRef](#)]
27. González-Tello, P.; Camacho, F.; Vicaria, J.M.; González, P.A. A modified Nukiyama–Tanasawa distribution function and a Rosin–Rammler model for the particle-size-distribution analysis. *Powder Technol.* **2008**, *186*, 278–281. [[CrossRef](#)]
28. Wan, G.; Sun, G.; Xue, X.; Shi, M. Solids concentration simulation of different size particles in a cyclone separator. *Powder Technol.* **2008**, *183*, 94–104. [[CrossRef](#)]
29. Xu, H.; Zhang, P.; Hu, Z.; Mao, E.; You, Z.; Du, Y. Analysis of dust emission characteristics of peanut whole-feed harvesting based on total amount collection method. *Int. J. Environ. Res. Public Health* **2022**, *19*, 15937. [[CrossRef](#)]
30. Qian, J.; Ferro, A.R.; Fowler, K.R. Estimating the resuspension rate and residence time of indoor particles. *J. Air Waste Manag. Assoc.* **2012**, *58*, 502–516. [[CrossRef](#)]
31. Stacey, P.; Thorpe, A.; Roberts, P.; Butler, O. Determination of respirable-sized crystalline silica in different ambient environments in the United Kingdom with a mobile high flow rate sampler utilising porous foams to achieve the required particle size selection. *Atmos. Environ.* **2018**, *182*, 51–57. [[CrossRef](#)]

Disclaimer/Publisher’s Note: The statements, opinions and data contained in all publications are solely those of the individual author(s) and contributor(s) and not of MDPI and/or the editor(s). MDPI and/or the editor(s) disclaim responsibility for any injury to people or property resulting from any ideas, methods, instructions or products referred to in the content.